Article

Thermally Reduced Ruthenium Nanoparticles as a Highly Active Heterogeneous Catalyst for Hydrogenation of Monoaromatics

Fabing Su, Lu Lv, Fang Yin Lee, Tao Liu, Andrew I. Cooper, and Xiu Song Zhao

J. Am. Chem. Soc., **2007**, 129 (46), 14213-14223• DOI: 10.1021/ja072697v • Publication Date (Web): 31 October 2007

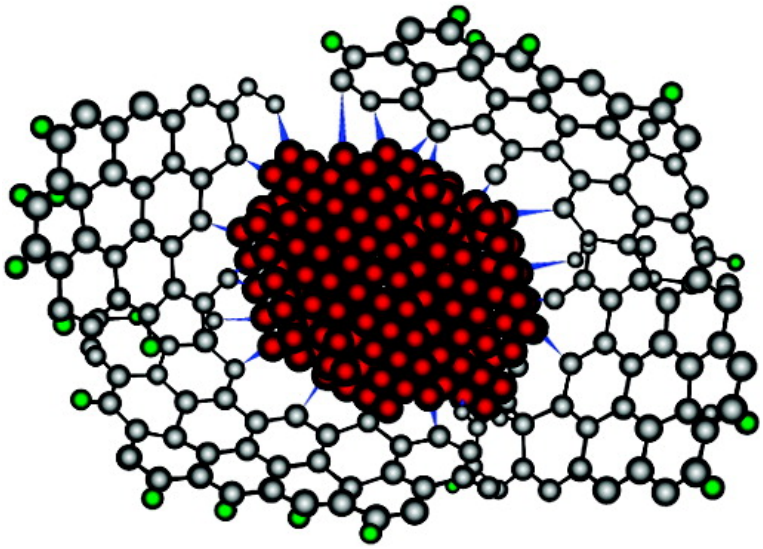

J|A|C|S
ARTICLES
Published on Web 10/31/2007

Thermally Reduced Ruthenium Nanoparticles as a Highly Active Heterogeneous Catalyst for Hydrogenation of Monoaromatics

Fabing Su,*[,†,‡] Lu Lv,[†] Fang Yin Lee,[§] Tao Liu,[||] Andrew I. Cooper,[‡] and Xiu Song Zhao*[,†,§]

Contribution from the Department of Chemical and Biomolecular Engineering, National University of Singapore, 4 Engineering Drive 4, Singapore 117576, Department of Chemistry, University of Liverpool, Crown Street, Liverpool L69 3BX, United Kingdom, Nanoscience and Nanotechnology Initiative, National University of Singapore, 2 Engineering Drive 3, Singapore 117576, and Physics Department, National University of Singapore, 2 Science Drive 3, Singapore 117542

Received April 24, 2007; E-mail: fabing.su@liverpool.ac.uk; chezxs@nus.edu.sg

Abstract: We report here a thermal reduction method for preparing Ru catalysts supported on a carbon substrate. Mesoporous SBA-15 silica, surface-carbon-coated SBA-15, templated mesoporous carbon, activated carbon, and carbon black with different pore structures and compositions were employed as catalyst supports to explore the versatility of the thermal reduction method. Nitrogen adsorption, X-ray diffraction, field-emission scanning electron microscopy, transmission electron microscopy, scanning transmission electron microscopy, thermogravimetric analysis, and X-ray absorption near-edge structure techniques were used to characterize the samples. It was observed that carbon species that could thermally reduce Ru species at high temperatures played a vital role in the reduction process. Ru nanoparticles supported on various carbon-based substrates exhibited good dispersion with an appropriate particle size, high crystallinity, strong resistance against oxidative atmosphere, less leaching, lack of aggregation, and avoidance of pore blocking. As such, these catalysts display a remarkably high catalytic activity and stability in the hydrogenation of benzene and toluene (up to 3−24-fold compared with Ru catalysts prepared by traditional methods). It is believed that the excellent catalytic performance of the thermally reduced Ru nanoparticles is related to the intimate interfacial contact between the Ru nanoparticles and the carbon support.

1. Introduction

High-performance heterogeneous catalysts are increasingly in demand for clean technology and sustainable development. Precious metals such as Pt, Ru, Pd, and Rh are used widely as catalysts in automotive-emission control systems, chemical industries, and fuel cell devices. High demand for these scarce metals has led to their serious shortage and rapid cost increase. Therefore, recent research effort has focused strongly on maximizing the catalytic efficiency of the precious metal catalysts by optimizing their physicochemical properties,[1] forming alloy structures,[2] developing new catalyst supports,[3] adding promoters,[4] and modifying the metal−support interactions.[5]

Both heterogeneous[6] and homogeneous ruthenium catalysts[7] have been used in hydrogenation reactions for several decades. The heterogeneous catalyst system is preferred from both industrial and environmental standpoints. Ru nanoparticles supported on mesoporous silicas,[8] hydroxyapatites,[9] porous carbons,[10,11] zeolite β,[12] alumina,[13] and titanium oxides[13] have been reported to be highly active for various reactions. Heterogeneous Ru catalysts are traditionally prepared by

[†] Department of Chemical and Biomolecular Engineering, National University of Singapore.
[‡] Department of Chemistry, University of Liverpool.
[§] Nanoscience and Nanotechnology Initiative, National University of Singapore.
[||] Physics Department, National University of Singapore.

(1) (a) Bell, A. T. *Science* **2003**, *299*, 1688. (b) Zhang, J.; Sasaki, K.; Sutter, E.; Adzic, R. R. *Science* **2007**, *315*, 220. (c) Stamenkovic, V. R.; Fowler, B.; Mun, B. S.; Wang, G.; Ross, P. N.; Lucas, C. A.; Marković, N. M. *Science* **2007**, *315*, 493.
(2) Enache, D. I.; Edwards, J. K.; Landon, P.; Solsona-Espriu, B.; Carley, A. F.; Herzing, A. A.; Watanabe, M.; Kiely, C. J.; Knight, D. W.; Hutchings, G. J. *Science* **2006**, *311*, 362.
(3) Joo, S. H.; Choi, S. J.; Oh, I.; Kwak, J.; Liu, Z.; Terasaki, O.; Ryoo, R. *Nature* **2001**, *412*, 169.
(4) Hansen, T. W.; Wagner, J. B.; Hansen, P. L.; Dahl, S.; Topsøe, H.; Jacobsen, C. J. H. *Science* **2001**, *294*, 1508.
(5) (a) Fu, Q.; Saltsburg, H.; Flytzani-Stephanopoulos, M. *Science*, **2003**, *301*, 935. (b) Kang, J. H.; Menard, L. D.; Nuzzo, R. G.; Frenkel, A. I. *J. Am. Chem. Soc.* **2006**, *128*, 12068.
(6) Carnahan, J. E.; Ford, T. A.; Gresham, W. F.; Grigsby, W. E.; Hager, G. F. J. *Am. Chem. Soc.* **1955**, *77*, 3766.
(7) Evans, D.; Osborn, J. A.; Jardine, F. H.; Wilkinson, G. *Nature* **1965**, *208*, 1203.
(8) (a) Zhou, W.; Thomas, J. M.; Shephard, D. S.; Johnson, B. F. G.; Ozkaya, D.; Maschmeyer, T.; Bell, R. G.; Ge, Q. *Science* **1998**, *280*, 705. (b) Kluson, P.; Had, J.; Belohlav, Z.; Cerveny, L. *Appl. Catal., A* **1997**, *149*, 331. (c) Hulea, V.; Brunel, D.; Galarneau, A.; Philippot, K.; Chaudret, B.; Kooyman, P. J.; Fajula, F. *Microporous Mesoporous Mater.* **2005**, *79*, 185.
(9) Ho, C.-M.; Yu, W. Y.; Che. C.-M. *Angew. Chem., Int. Ed.* **2004**, *43*, 3303.
(10) (a) van Gorp, K.; Boerman, E.; Cavenaghi, C. V.; Berben, P. H. *Catal. Today* **1999**, *52*, 349. (b) Zhanga, Z.; Jackson, J. E.; Miller, D. J. *Appl. Catal. A.* **2001**, *219*, 89. (c) Liang, C.; Wei, Z.; Xin, Q.; Li, C. *Appl. Catal., A* **2001**, *208*, 193.

impregnation of a Ru precursor on the surface of a porous solid support followed by hydrogen reduction (in gas) or chemical reduction (normally in liquid).[14] These common methods tend to lead to relatively weak interactions between the Ru particles and the support.[15] Hence, partial oxidation, aggregation/sintering, and leaching of Ru particles are the problems frequently encountered in catalyst preparation and use.

Recently, Miao and co-workers reported the immobilization of Ru particles on montmorillonite clay (Ru/MMT) with the assistance of ionic liquids.[16] While the Ru/MMT catalyst exhibited an excellent activity in the hydrogenation of benzene because of the strong synergistic interaction or Ru particles with support, the Ru nanoparticles were found to be slightly oxidized and to aggregate to form larger particles after several reaction runs. Sun et al.[17] reported the deposition of Ru colloidal nanoparticles on carbon nanotubes in supercritical water. However, the use of carbon nanotubes as a catalyst support could be limited because of their low surface area and high cost.

The hard template strategy[18] offers great opportunities for preparing novel catalysts.[19] In general, a mixture of metal and carbon precursors is first impregnated into the pores of a porous material (hard template), followed by carbonization and removal of the template. However, such a template strategy results in inaccessibility of some of the metal nanoparticles because they are occluded in the carbon matrix. Additionally, removal of the hard template using chemicals such as HF and/or NaOH raises environmental and manufacture cost issues. In a recent paper, we showed that Ru nanoparticles could be sandwiched in a matrix of porous carbon via chemical vapor deposition methods and that these materials displayed high catalytic activity and stability.[20] Although the method is relatively complicated and impractical for industrial use, the results suggested that intimate Ru−carbon contact could substantially improve the catalytic properties of Ru particles. More recent studies showed that electron-deficient concave surfaces and nanospace confinement could influence the synergetic interaction of metal nanoparticles with carbon supports.[21−23] On the basis of these rational results, further improvement in the catalytic properties of Ru heterogeneous catalysts seems possible.

In this paper, we demonstrate a thermal reduction method for preparing novel Ru heterogeneous catalyst, which exhibited a remarkably high catalytic activity, stability, and reusability for the hydrogenation of monoaromatics (benzene and toluene). The hydrogenation reactions represent model reactions for catalytic transformations of other aromatics and are also significant in the production of high-quality diesel fuels.[24] In contrast to more traditional catalyst preparation methods, the thermal reduction method described here utilizes carbon species as the reducing agent for Ru precursors at high temperatures, thereby leading to good particle dispersion of Ru nanoparticles with appropriate particle sizes, high crystallinity, strong resistance against oxidative atmospheres, reduced leaching, lack of aggregation, and retention of the pore structure in the support (namely, avoidance of pore blocking by agglomerates).

2. Experimental Section

2.1. Catalyst Supports. (1) Mesoporous pure-silica SBA-15 (denoted as silica) was synthesized according to Zhao et al.[25](2) Surface-carbon-coated SBA-15 silica (designated as C-silica): To coat a layer of carbon on the pore surface of SBA-15, 2 mL of deionized water containing sucrose (0.20 g) and H_2SO_4 (0.04 g) was stirred with SBA-15 (0.50 g) for 4 h. After being dried at 120 °C overnight, the solid was carbonized at 900 °C for 2 h under nitrogen to form C-silica. (3) Templated mesoporous carbon (TMC): The detailed preparation was described elsewhere.[26] (4) Activated carbons: A powdery activated carbon (designated as AC1) commercially known as SAE SUPER and produced from coal was purchased from NORIT (Norit Singapore Pte. Ltd.). A granular activated carbon (designated as AC2; sold commercially as GCN 1240 and prepared from coconut shells) was purchased from the same supplier. AC2 was pulverized into powder before use. (5) Carbon black (Vulcan XC-72) was purchased from Cabot Corp.

2.2. Preparation of Supported Ru Catalysts. (1) Catalyst Ru/silica-H: Silica (0.50 g) was impregnated with 2 mL of an aqueous solution containing 0.075 g of ruthenium chloride hydrate ($RuCl_3 \cdot H_2O$, Aldrich). After evaporation at 100 °C and drying at 200 °C for 3 h, hydrogen reduction was conducted at 400 °C for 2 h to obtain catalyst Ru/silica-H,[12,13] in which "H" denotes hydrogen reduction (also throughout text). (2) Catalysts Ru/C-silica-H and Ru/TMC-H: 0.50 g portions of supports C-silica and TMC were impregnated with 2 mL of an aqueous solution containing 0.065 g of $RuCl_3 \cdot H_2O$ followed by evaporation and drying at 150 °C for 3 h. Hydrogen reduction was carried out at 300 °C for 2 h to obtain catalysts Ru/C-silica-H and Ru/TMC-H.[11] (3) Catalysts Ru/C-silica and Ru/TMC: 0.50 g of C-silica and TMC were impregnated with 2 mL of an aqueous solution containing 0.065 g of $RuCl_3 \cdot H_2O$ followed by evaporation and drying at 150 °C for 3 h. The solid was then treated at 900 °C for 2 h under nitrogen (99.999%) atmosphere, during which Ru species were thermally reduced to Ru nanoparticles. This catalyst preparation method is referred to throughout as the thermal reduction method. (4) Catalysts Ru/C-silica-AH and Ru/TMC-AH: Catalysts Ru/C-silica and Ru/TMC prepared above were further calcined in air at 200 °C for 2 h to yield samples Ru/C-silica-A and Ru/TMC-A, respectively (here "A" means air oxidation), followed by hydrogen reduction at 300 °C for 2 h to obtained Ru/C-silica-AH and Ru/TMC-AH catalysts. (5) Catalysts Ru/AC1-H, Ru/AC1, Ru/AC2-H, and Ru/AC2: These catalysts were prepared using the methods similar to that for catalysts Ru/TMC-H and Ru/TMC. The only difference was that activated carbons AC1 and AC2 were used as the

(11) (a) Gallezot, P.; Nicolaus, N.; Flèche, G.; Fuertes, P.; Perrard, A. *J. Catal.* **1998**, *180*, 51. (b) Fabre, L.; Gallezot, P.; Perrard, A. *J. Catal.* **2002**, *208*, 247. (c) Cerro-Alarcón, M.; Maroto-Valiente, A.; Rodríguez-Ramos, I.; Guerrero-Ruiz, A. *Carbon* **2005**, *43*, 2711. (d) Crezee, E.; Hoffer, B. W.; Berger, R. J.; Makkee, M.; Kapteijn, F.; Jacob, A.; Moulijn, J. A. *Appl. Catal., A* **2003**, *251*, 1.
(12) Kantam, M. L.; Rao, B. P. C.; Choudary, B. M.; Sreedhara. B. *Adv. Synth. Catal.* **2006**, *348*, 1970.
(13) Kusserow, B.; Schimpf, S.; Claus, P. *Adv. Synth. Catal.* **2003**, *345*, 289.
(14) Kluson, P.; Cerveny, L. *Appl. Catal., A* **1995**, *128*, 13.
(15) Augustin, R. L. *Heterogeneous catalysis for the synthetic chemistry*; Marcel Dekker, Inc.: New York, 1995; pp 169−175.
(16) Miao, S.; Liu, Z.; Han, B.; Huang, J.; Sun, Z.; Zhang, J.; Jiang, T. *Angew. Chem., Int. Ed.* **2006**, *45*, 266.
(17) Sun, Z.; Liu, Z.; Han, B.; Wang, Y.; Du, J.; Xie, Z.; Han, G. *Adv. Mater.* **2005**, *17*, 928.
(18) (a) Lu, A.-H.; Schüth, F. *Adv. Mater.* **2006**, *18*, 1793. (b) Su, F.; Zhou, Z.; Guo, W.; Liu, J.; Tian, X. N.; Zhao, X. S. *Chemistry and Physics of Carbon*; Radovic, L. R., Ed.; Marcel Dekker: New York, 2007; Vol. 30, Chapter 2.
(19) (a) Choi, W. C.; Woo, S. I.; Jeon, M. K.; Sohn, J. M.; Kim, M. R.; Jeon, H. J. *Adv. Mater.* **2005**, *17*, 446. (b) Liu, S.-H.; Lu, R.-F.; Huang, S.-J.; Lo, A.-Y.; Chien, S.-H.; Liu, S.-B. *Chem. Commun.* **2006**, 3435. (c) Ikeda, S.; Ishino, S.; Harada, T.; Okamoto, N.; Sakata, T.; Mori, H.; Kuwabata, S.; Torimoto, T.; Matsumura, M. *Angew. Chem., Int. Ed.* **2006**, *45*, 7063. (d) Lu, A.-H.; Li, W.-C.; Hou, Z.; Schüth, F. *Chem. Commun.* **2007**, 1038.
(20) Su, F.; Lee, F.; Lv, L.; Liu, J.; Tian, X. N.; Zhao, X. S. *Adv. Funct. Mater.* **2007**, *17*, 1926.
(21) Duca, D.; Ferrante, F.; Manna, G. L. *J. Phys. Chem. C* **2007**, *111*, 5402.
(22) Pan, X.; Fan, Z.; Chen, W.; Ding, Y.; Luo, H.; Bao, X. *Nat. Mater.* **2007**, *6*, 507.
(23) (a) Chen, W.; Pan, X.; Willinger, M. G.; Su, D. S.; Bao, X. *J. Am. Chem. Soc.* **2006**, *128*, 3136. (b) Chen, W.; Pan, X.; Bao, X. *J. Am. Chem. Soc.* **2007**, *129*, 7421.
(24) Roucoux, A.; Schulz, J.; Patin, H. *Chem. Rev.* **2002**, *102*, 3757.
(25) Zhao, D.; Feng, J.; Huo, Q.; Melosh, N.; Fredrickson, G. H.; Chmelka, B. F.; Stucky, G. D. *Science* **1998**, *279*, 548.
(26) Jun, S.; Joo, S. H.; Ryoo, R.; Kruk, M.; Jaroniec, M.; Liu, Z.; Ohsuna, T.; Terasaki, O. *J. Am. Chem. Soc.* **2000**, *122*, 10712.

supports instead of TMC. (6) Catalysts Ru/XC-H and Ru/XC: These two catalysts were prepared using methods similar to those described above for catalysts Ru/TMC-H and Ru/TMC. (7) Catalyst RuC/silica: 0.50 g of silica was impregnated with 2 mL of an aqueous solution containing 0.065 g of $RuCl_3 \cdot H_2O$ and 0.20 g sucrose followed by evaporation and drying at 150 °C for 3 h. The solid was then treated at 900 °C for 2 h under nitrogen. (8) Composite RuO_2/silica: For comparison, 0.50 g of silica was impregnated with 2 mL of an aqueous solution containing 0.075 g of $RuCl_3 \cdot H_2O$. After evaporation and drying at 150 °C for 3 h, the sample was treated at 900 °C for 2 h under a nitrogen atmosphere.

The mass content of Ru in each catalyst was evaluated on the basis of the $RuCl_3 \cdot H_2O$ added and the total mass of the final catalyst obtained. It should be noted that hydrogen reduction of Ru on carbon surfaces cannot be carried out at 900 °C because methanation and gasification of carbon catalyzed by Ru species commences at about 400 °C.[27] Our experimental data also showed complete gasification of carbon at 900 °C in the presence of Ru.

2.3. Characterization Techniques. The porous properties of the supports were investigated using physical adsorption of nitrogen at 77.3 K using an automatic volumetric sorption analyzer (Quantachrome, NOVA1200). Prior to the measurement, the samples were degassed at 200 °C for 5 h under vacuum (10^{-2} mmHg). The specific surface areas were determined according to the Brunauer−Emmett−Teller (BET) method in the relative pressure range 0.05−0.20. Total pore volumes were obtained from the volume of nitrogen adsorbed at a relative pressure of 0.99. The pore size distribution (PSD) curves were derived using the Barrett−Joyner−Halenda (BJH) method from the adsorption branches. The pore sizes were estimated from the peak positions of the BJH−PSD curves. X-ray diffraction (XRD) patterns were collected on an XRD-6000 (Shimadzu, Kyoto, Japan) with Cu Kα radiation of wavelength $\lambda = 0.154\ 18$ nm. Thermogravimetric analysis (TGA) was conducted on a thermogravimetric analyzer TGA 2050 (TA Instruments, New Castle, DE) in air with a flow rate of 100 mL/min and a temperature ramp of 10 °C/min. The microscopic features of the samples were observed with a field-emission scanning electron microscope (FESEM) (JSM-6700F, JEOL, Tokyo, Japan) operated at 10 kV, field-emission transmission electron microscope (FETEM) (JEM 2010F, JEOL, Tokyo, Japan) operated at 200 kV, and scanning transmission electron microscope (STEM) (JSM-6700F equipped with transmission electron detector) operated at 25 kV. X-ray absorption near edge structure (XANES) experiments at the Ru L_3-edge (2.838 keV) were performed at room temperature at the XDD beamline in the Singapore Synchrotron Light Source (SSLS),[28] where a pair of channel-cut Si-(111) crystals was used in the monochromator. All spectra were collected in transmission mode where two ionization chambers filled with nitrogen were employed to record the incident and transmitted X-ray intensities. The high-order harmonic components in the incident beam were not suppressed effectively due to the design of channel-cut monochromator. We assumed that this had the same effect on XANES for all samples, and we therefore focus on the trends observed throughout the series of samples. The spectrum of argon gas was recorded for energy calibration.[29] The spectra were measured from 2750 to 2950 eV with an energy step of 1 eV in the pre- and postedge region and 0.15 eV at the edge regime. Linear fits to the pre- and postedge regime were performed for background removal and normalization.

Catalyst leaching experiments were carried out as follows: Around 0.10 g of fresh or one-reaction-run Ru catalyst was placed in 10 mL of water under shaking for 4 days at 200 rpm. After filtration of the suspension, the Ru concentration in the solution was determined using an inductive-coupled plasma atomic mass spectrometer (ICP-MS) on a Perkin-Elmer ELAN6100 at a wavelength of 100.9 nm.[20]

H_2 chemisorption on Ru catalysts was attempted to measure using various methods such as Micromeritics AutoChem II 2920 automated catalyst characterization system, Micromeritics ASAP2050 high-pressure hydrogen adsorption system, and microcalorimetry. However, we did not observe the H_2 chemisorption. The reason for this is not clear at present.

2.4. Measurement of Catalytic Activities. The catalytic properties of the Ru catalysts for monoaromatics hydrogenation (benzene and toluene) were evaluated using a 300-mL stainless-steel batch reactor (Parr Instruments). A given amount of Ru catalyst and 30 mL of benzene or toluene (99.9%, Aldrich) were placed in the reactor. Subsequently, the reactor was purged with high purity H_2 (>99.99%, Singapore Oxygen Air Liquide Pte. Ltd.) for 5 min. Next, the reaction pressure was generated using H_2 at the reaction temperature. The reaction system was stirred at 300 rpm, and the pressure was kept constant. After no uptake of H_2 was observed (by monitoring the system pressure and temperature), the reactor was cooled to room temperature in an ice−water bath and the pressure in the reactor was released. To investigate the recyclability of the catalyst, the used Ru catalyst was filtered after the reaction and vacuum-dried at 80 °C overnight before the next reaction run. The product liquid in reactor was analyzed using an isocratic high-performance liquid chromatograph (Agilent 1100 series HPLC) system with an Agilent 1100 standard variable wavelength UV detector and an AD-H normal phase column (250 × 4.6 mm, 5 μm packing size, Daicel Chemical Industries). The concentrations of the monoaromatics were quantified at a wavelength of 254 nm on the basis of a standard calibration curve constructed prior to the quantitative analysis using an eluent of 95% *n*-hexane plus 5% isopropyl alcohol at a flow rate of 1 mL/min under isobaric conditions. The mean catalytic activity of a catalyst was calculated as the conversion of mol of benzene (or toluene)/(mol of Ru/h),[16,20] which could be used directly to compare the efficiency of the various catalysts.

3. Results

3.1. Characterization of the Supports Using N_2 Adsorption. Figure 1 shows the N_2 adsorption−desorption isotherms for the catalyst supports used in this work. It can be seen from Figure 1a that silica displays a type IV isotherm with an H1 hysteresis loop, indicating that it is mesoporous with relatively uniform mesopores centered at 7.9 nm, as shown in PSD curve (inset, Figure 1a). The composite C-silica also shows a type IV isotherm and H1 hysteresis loop (Figure 1b) and is mesoporous material with an average pore size of around 6.3 nm (inset). The smaller average pore size with respect to silica results from the carbon film coated on the pore surface of the silica as well as shrinkage of silica which occurs at high temperatures.[30] The templated mesoporous carbon (TMC) in Figure 1c reveals a type IV isotherm with a H2 hysteresis loop and a uniform pore size centered at 4.1 nm, consistent with previous reports.[26] TMC has been demonstrated to be a good support for exploring novel heterogeneous catalyst systems and for fundamental studies.[3,30,31] The isotherm of activated carbon AC1 (Figure 1d) is of type I, and the stepwise increase in the adsorption branch and wide PSD demonstrates the presence of both micropores and mesopores. By contrast, Figure 1e shows type I isotherm for AC2

(27) Koopman, P. G. J.; Kieboom, A. P. G.; van Bekkum, H.; Coenen, J. W. E. *Carbon* **1979**, *17*, 399.
(28) Moser, H. O.; et al. *Nucl. Instrum. Methods Phys. Res., Sect. B* **2005**, *238*, 83.
(29) Brendebach, B.; Bucher, S.; Hormes, J.; Bönnemann, H.; Nagabhushana, K. S.; Brinkmann, R.; Modrow, H. *Phys. Scr.* **2005**, *T115*, 773.
(30) Su, F.; Zeng, J.; Bao, X.; Yu, Y.; Lee, J. Y.; Zhao, X. S. *Chem. Mater.* **2005**, *17*, 3960.
(31) (a) Lu, A. -H.; Schmidt, W.; Matoussevitch, N.; Bönnemann, H.; Spliethoff, B.; Tesche, B.; Bill, E.; Kiefer, W.; Schüth, F. *Angew. Chem., Int. Ed.* **2004**, *43*, 4303. (b) Li, L.; Zhu, Z. H.; Lu, G. Q.; Yan, Z. F.; Qiao, S. Z. *Carbon* **2007**, *45*, 11. (c) Wang, Y.; Cheng, L.; Li, F.; Xiong, H.; Xia, Y. *Chem. Mater.* **2007**, *19*, 2095. (d) Cui, G.; Zhi, L.; Thomas, A.; Kolb, U.; Lieberwirth, I.; Müllen, K. *Angew. Chem., Int. Ed.* **2007**, *46*, 3464.

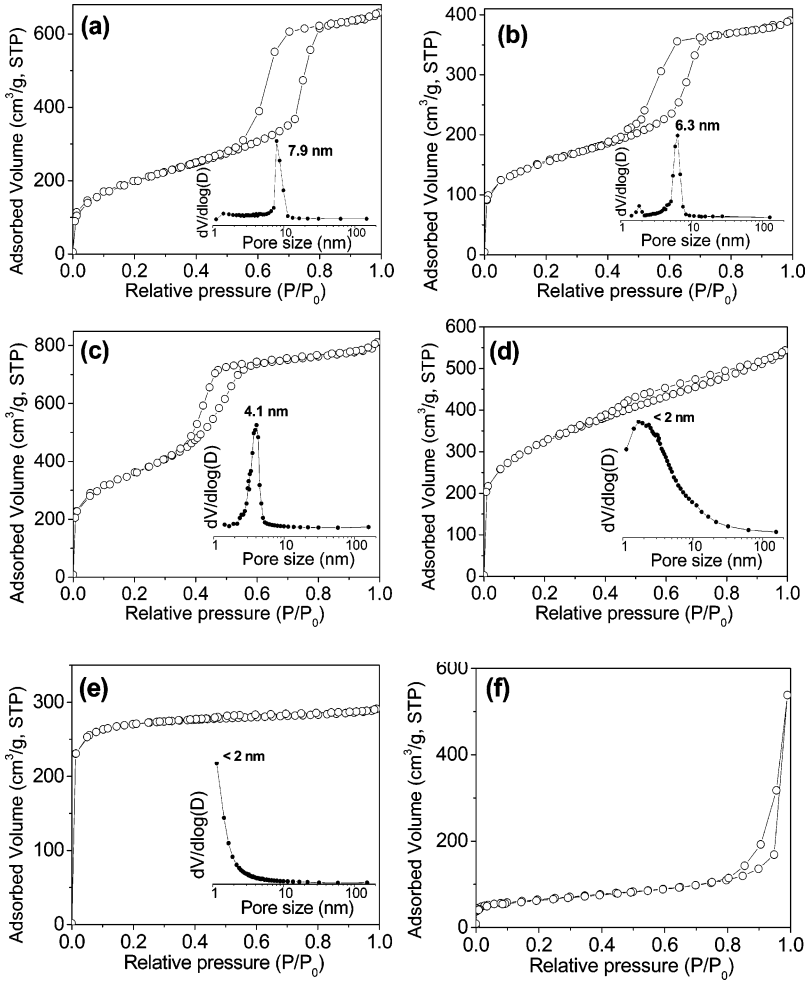

Figure 1. N_2 adsorption−desorption isotherms and PSD (inset) for the catalyst supports used in this work: (a) silica; (b) C-silica; (c) TMC; (d) AC1; (e) AC2; (f) XC-72.

with a flat profile in the adsorption branch and a narrow PSD curve (inset), indicating a predominance of micropores. Figure 1f shows a type III isotherm for carbon black XC-72, in keeping with its nonporous structure. It has been known that XC-72 is composed of carbon nanoparticles with diameters in the range 50−100 nm and the material has been used widely in electrocatalyst supports. The detailed parameters for these supports are compiled in Table 1, which lists the different pore structures for the supports used in this work.

3.2. Characterization of the Ru Catalysts. Table 1 and Figure S1 (see Supporting Information) show that the pore structures of the thermally reduced and hydrogen-reduced Ru catalysts are consistent with the respective parent porous supports.

Figure 2 shows STEM images of Ru/silica-H, Ru/C-silica-H, and Ru/C-silica catalysts at different magnifications. The Ru nanoparticles in the Ru/silica-H catalyst (Figure 2a,b) can be observed as dark dots dispersed within the array of pore channels in the silica support. Slight aggregation of some nanoparticles was also observed in the pore channels. The Ru nanoparticle size was observed to be around 5−7 nm (Figure 2b), consistent with the pore channel diameter and the confinement within the channel space. Similarly, Figure 2c,d shows that the Ru nanoparticles in the Ru/C-silica-H catalyst are highly distributed within the pore channels of the C-silica support. However, the Ru nanoparticle size in Figure 2d is smaller than that of Ru/silica-H (Figure 2b), possibly because of the lower hydrogen reduction temperature and different support surface properties. For the Ru/C-silica catalyst, Ru nanoparticles were also uniformly dispersed within the support and no particle aggregation was observed (Figure 2e,f). In particular, no large Ru nanoparticles were observed on the external surface of the support (Figure 2f) even though the thermal reduction process was conducted at high-temperature (900 °C). Interestingly, the

Table 1. Pore Structure Parameters of Various Supports and Catalysts

sample	surf area (m^2/g)	pore vol (cm^3/g)	pore size (nm)
silica	711	1.01	7.9
C-silica	534	0.60	6.3
TMC	1305	1.27	4.1
AC1	1090	0.84	<2
AC2	860	0.45	<2
XC-72	220		
Ru/silica-H	644	0.90	7.5
Ru/C-silica	490	0.44	6.1
Ru/C-silica-H	495	0.59	6.2
Ru/TMC	1070	0.76	3.6
Ru/TMC-H	1240	1.21	4.1
Ru/AC1	1002	0.55	<2
Ru/AC1-H	1052	0.78	<2
Ru/AC2	808	0.40	<2
Ru/AC2-H	830	0.43	<2

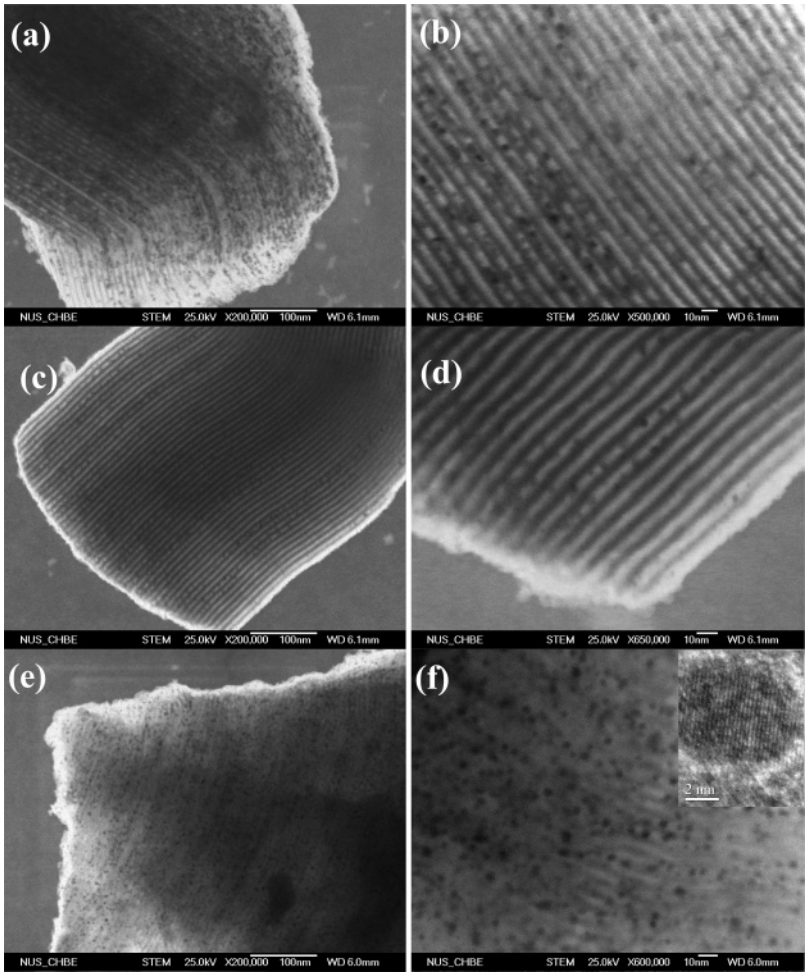

Figure 2. STEM images at different magnifications: (a, b) Ru/silica-H; (c, d) Ru/C-silica-H; (e, f) Ru/C-silica. The inset of (f) shows the TEM image of a single Ru nanoparticle in the Ru/C-silica.

Ru nanoparticle diameter in the Ru/C-silica sample (Figure 2f) was about 5−7 nm which is comparable to the Ru/silica-H material. The inset in Figure 2f shows a TEM image of a single Ru nanoparticle taken in the Ru/C-silica sample, displaying aligned crystal lattices with an average spacing of about 0.21 nm; this corresponds to the (101) plane of a Ru single crystal.[4]

Figures 3a,b show TEM images of the hydrogen-reduced Ru/TMC-H catalyst. Uniform pore channels templated from the silica are apparent, but it is difficult to distinguish clearly the Ru nanoparticles, even in the image at a higher magnification (Figure 3b). By contrast, for the thermally reduced Ru/TMC catalyst, Ru nanoparticles in the size range 1−5 nm were observed (Figure 3c,d). It is also noted that these nanoparticles were not located within pore channels but incorporated or semiembedded within the carbon nanorod framework: this differs from Ru/C-silica, as shown in Figure 2f. This difference arises from the thermal reduction process where the consumption of carbon in reducing the Ru particles lets them sit in or become embedded in the carbon substrate. The inset of Figure 3d shows a Ru nanoparticle with diameter of around 5 nm embedded in the carbon substrate. The aligned crystal lattices with an average spacing of about 0.21 nm also correspond to the (101) Ru crystal plane.[4] Figure 3e,f shows STEM images of Ru/XC-H and Ru/XC catalysts, respectively. The Ru nanoparticles in the latter material are clearly larger than in the former, again supporting the trend that thermally reduced Ru nanoparticles are larger than hydrogen-reduced in these systems. The formation of larger Ru particles in Ru/XC compared with Ru/TMC is possibly due to the difference in the carbon support properties (porosity and surface chemistry).

Figure 4a,b shows STEM images of Ru/C-silica-AH. It can be seen that, after calcination in air at 200 °C and reduction with hydrogen, the Ru particles exhibit no obvious changes compared with the counterpart Ru/C-silica (Figure 2e,f). Figure 4c,d shows TEM images of Ru/TMC-AH. Similarly, no significant observed differences are observed in comparison with Ru/TMC (Figure 3c,d). These images indicate that the treatment here for both catalysts does not lead to obvious alterations in the Ru particle morphology. The purpose of this treatment will be discussed below.

Figure 5 shows XRD patterns for various samples. Only one wide peak at around 23.1 degrees (2θ) in pattern a for C-silica was observed, which may be due to the amorphous or noncrystalline structure of silica and/or coated carbon diffraction (002). The XRD pattern of Ru/C-silica-H in pattern b shows a weak new peak at around 43.8° that corresponds to the (101) diffraction of hexagonal Ru metal (ICDD-JCPDS Card No. 06-0663), indicating the reduction of Ru on the support. Similarly, XRD patterns for Ru/silica-H in pattern c and Ru/C-silica in pattern d also show the emergence of this peak at around 44°, demonstrating the presence of metallic Ru nanoparticles. Comparison of the breadth of the 101 diffraction peak in patterns

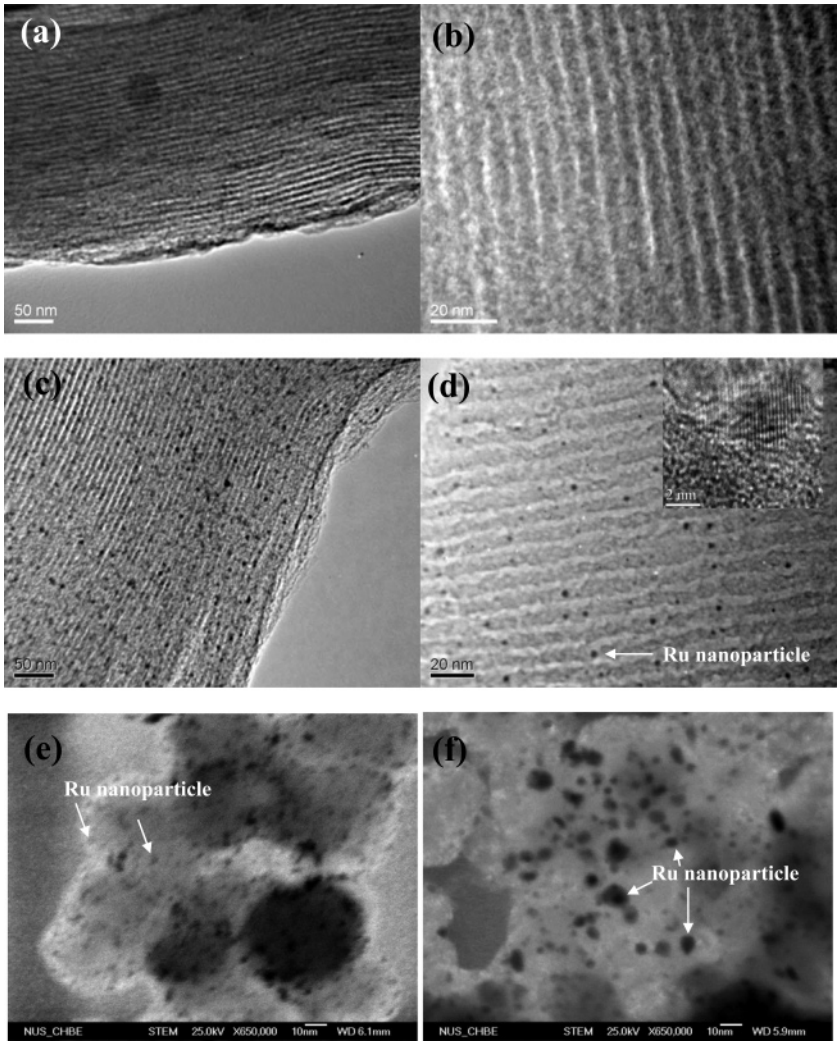

Figure 3. TEM images at different magnifications for (a, b) Ru/TMC-H and (c, d) Ru/TMC STEM images of (e) Ru/XC-H and (f) Ru/XC. The inset of (d) is a TEM image of a single Ru nanocrystal taken in Ru/TMC.

b−d gives an indirect indication of the crystal particle size and confirms that the Ru nanoparticle size in Ru/C-silica-H is smaller than that of Ru/silica-H and Ru/C-silica (which have comparable Ru nanoparticle size), as also observed by TEM observation (Figure 2). The peaks at around 28.1, 35.1, 44.0, and 54.4° observed in pattern e of Ru/C-silica-A and pattern f of RuO_2/silica can be indexed to the (110), (101), (111), and (211) diffractions of anhydrous crystalline RuO_2 (ICDD-JCPDS Card No. 43-1027) with a rutile-type structure. The XRD pattern of Ru/C-silica-A suggests the successful oxidation of Ru/C-silica under the calcination conditions used. Figure S2 shows TEM images of RuO_2/silica, revealing RuO_2 particles dispersed in pore channels of silica. Comparison of patterns d and f suggests that the coated carbon substrate on the surface of the silica plays a vital role as a reducing agent in the thermal reduction of Ru at high temperature in the absence of hydrogen gas.

Figure 6 compares the XRD patterns of TMC and carbon-supported Ru catalysts. The XRD pattern of TMC (pattern a) shows two broad peaks located at around 25 and 43°, corresponding to (002) and (101) diffractions of typical amorphous carbon, respectively. A very similar peak profile in pattern b implies the presence of very small Ru nanoparticles on Ru/TMC-H. In contrast, XRD patterns of Ru/TMC in pattern c shows a clear peak at 43.6° which overlaps with C(101) and Ru(101) diffractions, indicating the presence of relatively large Ru nanoparticles on Ru/TMC, in good agreement with TEM observations (Figure 3). Hydrogen-reduced Ru/XC-H in pattern d possesses a profile similar to that of Ru/TMC-H. For thermally reduced catalyst Ru/XC in pattern e, the peaks at 38.5, 42.3, 44.1, 58.4, 69.6, and 78.5° can be assigned respectively to (100), (002), (101), (102), (110), and (103) diffractions of bulk hexagonal Ru metal (ICDD-JCPDS Card No. 06-0663). The relatively sharp profile of the Ru(101) peak is due to the large Ru particles formed on the external surface of the nonporous carbon black XC-72, while the broad base stems from small nanoparticles, implying that the Ru particles are not uniform, in agreement with STEM observations (Figure 3f). These results clearly demonstrate that the thermally reduced Ru nanoparticles have a high crystallinity. No diffraction peak at around 35° was observed for the thermally reduced Ru catalysts, demonstrating the efficiency of the thermal reduction method.

Figure 7 shows TGA for Ru/C-silica, Ru/TMC, and TMC. It can be seen that the residual weight of Ru/C-silica in air was around 90.6 wt % above 600 °C, suggesting that the coated carbon content was around 9.4 wt %. The residual weight for Ru/TMC above 550 °C was about 7.7 wt % (RuO_2) in keeping with the complete removal of the silica template in TMC.[30] Thus, the Ru content in Ru/TMC was calculated to be around

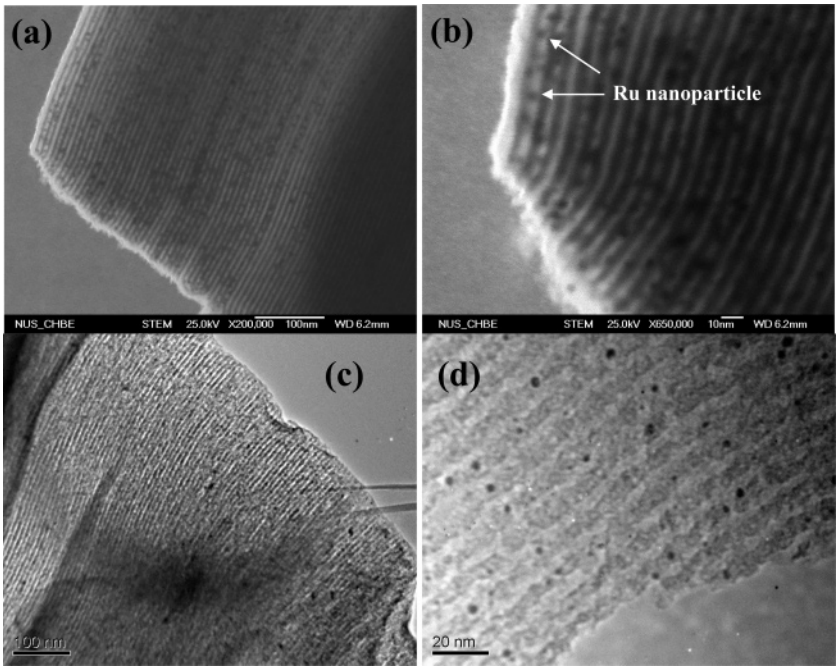

Figure 4. (a, b) STEM images of Ru/C-silica-AH at different magnifications and (c, d) TEM images of Ru/TMC-AH at different magnifications.

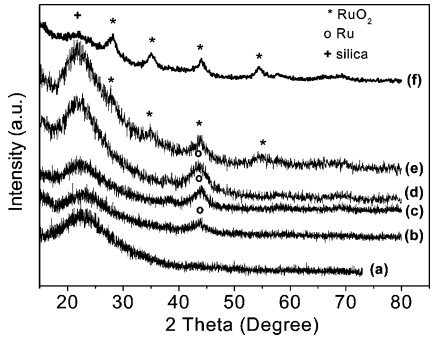

Figure 5. XRD patterns: (a) C-silica; (b) Ru/C-silica-H; (c) Ru/silica-H; (d) Ru/C-silica; (e) Ru/C-silica-A; (f) RuO_2/silica.

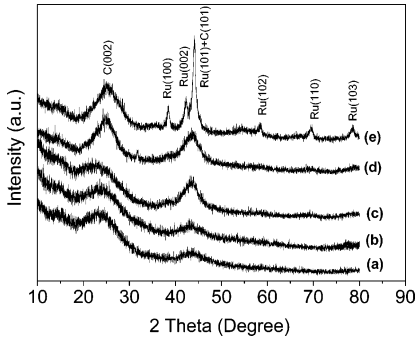

Figure 6. XRD patterns: (a) TMC; (b) Ru/TMC-H; (c) Ru/TMC; (d) Ru/XC-H; (e) Ru/XC.

6.0 wt %, consistent with ratio of Ru added to the final catalyst amount obtained (5.9 wt %). The TGA curve also indicates that the start point of carbon combustion for Ru/TMC was around 250 °C, much lower for TMC. The weight loss of Ru/TMC occurred mostly in the range 300−450 °C, also much lower than for TMC (500−650 °C), indicating catalytic combustion at lower temperatures in the presence of Ru oxides. Thus, to avoid combustion of the carbon support, we carried out mild oxidation of Ru for Ru/TMC and Ru/C-silica catalysts (air at

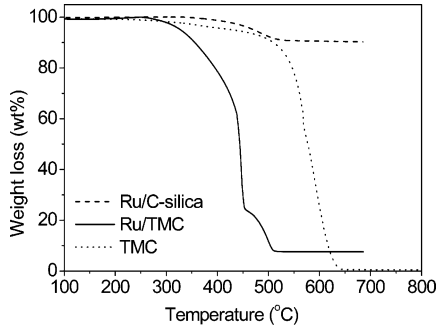

Figure 7. TGA curves of Ru/C-silica and Ru/TMC catalysts in air (heating rate: 10 °C/h).

200 °C for 2 h). The second weight loss of Ru/TMC in the range 450−500 °C was possibly derived from the oxidation of carbon species that were not in direct contact with the Ru oxides.

From the analysis above, it is still difficult to distinguish clearly in terms of chemical differences between the hydrogen-reduced and thermally reduced Ru nanoparticles, apart from the difference in average size. Ru L_3-edge XANES, which is a direct probe of the 4d-related final states of Ru, was therefore used to look for any differences in the oxidation states of the Ru atoms, which are related to charge transfer in the valence state. The Ru L_3-edge XANES spectra of the catalysts and reference samples are compared in Figure 8. Samples Ru/silica-H and RuO_2/silica were measured as reference compounds, representing Ru atoms in oxidation states of 0 and 4+ valence states, respectively, and labeled as "A" and "B" in Figure 8. Compared with the spectra of the catalyst Ru/silica-H, the shift of the absorption peak of RuO_2/silica toward higher energy is due to the increased valence states of Ru in these samples. The Ru/TMC-A and Ru/TMC-H samples showed two dominant absorption peaks: the sharper peak A at low-energy represents the presence of metallic Ru, and the broader peak B at high energy indicates Ru oxides if a comparison with the Ru/silica-H and RuO_2/silica "controls" is taken into account. The peak B for

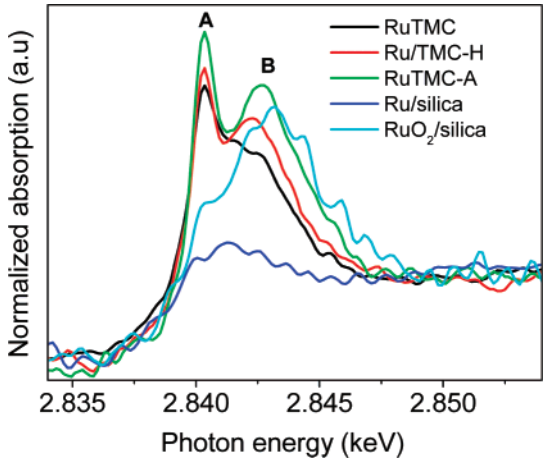

Figure 8. L_3-edge XANES spectra of Ru catalysts and reference compounds (Ru/silica-H and RuO_2/silica).

Ru/TMC-A is significant, indicating that this sample was partially oxidized due to the calcination in air at 200 °C for 2 h. Similarly, the lower intensity of this peak for Ru/TMC-H compared to that of Ru/TMC-A suggests that the Ru/TMC-H may be not fully reduced by hydrogen and/or easily oxidized when exposed in air. The lowest intensity of the peak B for thermally reduced Ru/TMC indicates that relatively complete thermal reduction at high-temperature (900 °C) was achieved, consistent with the XRD results in Figure 6. Thus, Ru/TMC catalyst has a relatively high degree of reduction and good stability against oxidation.

3.3. Catalytic Performance of the Ru Catalysts. Table 2 summarizes the catalytic properties of the Ru catalysts prepared in this study for benzene hydrogenation. The catalytic activity of Ru/C-silica (entry 1) is 18 times higher than that of Ru/silica-H (entry 2) and 13 times higher than that of Ru/C-silica-H (entry 3) even though the Ru nanoparticle size in Ru/C-silica is larger than that of Ru/C-silica-H and comparable to that of Ru/silica-H, as confirmed by STEM (Figure 2) and XRD (Figure 5). Additionally, the pore structures of these three catalysts are comparable (see Table 1 and Figure S1). This implies that factors other than Ru particle size and carbon substrate pore structure play a significant role in enhancing the activity. Similarly, the activity of Ru/TMC (entry 4) is 15 times higher than that of Ru/TMC-H (entry 5) in spite of the larger Ru nanoparticle size of the former (see Figures 3 and 6). Under the same reaction conditions (110 °C and 8 MPa), the activities of catalysts Ru/C-silica (entry 6, 3.77×10^4 h^{-1}) and Ru/TMC (entry 7, 3.33×10^4 h^{-1}) are 9 and 8 times respectively higher than that of the Ru/MMT catalyst (4.0×10^3 h^{-1}), which was reported recently in the literature,[16] irrespective of the catalyst particle size. In addition, thermally reduced Ru catalysts also displayed a much higher catalytic activity than sandwiched Ru−carbon catalysts.[20] For example, under reaction conditions of 110 °C and 4 MPa, the activity of Ru/TMC was about 4 times that of a sandwiched Ru catalyst (RuC2) reported previously[20] although both materials were prepared using a one-batch synthesized silica template and possess similar average particle sizes and morphologies.

Moreover, significantly enhanced catalytic activities were observed when commercial activated carbons and carbon black were used as the catalyst supports, as shown in Table 2. The benzene hydrogenation activity for thermally reduced Ru/AC1 (entry 8) was 24 times greater than hydrogen-reduced Ru/AC1-H (entry 9); Ru/AC2 (entry 10) was 9 times more active than Ru/AC2-H (entry 11), and Ru/XC (entry 12) was 3 times more active than Ru/XC-H (entry 13). This systematic variation in activity is possibly due to the difference in chemistry and pore structure of these carbon supports. For catalysts Ru/C-silica, Ru/TMC, and Ru/AC1, the low loss in catalytic activity observed after 5 runs (entries 14−16) demonstrated that they were highly stable and reusable catalyst systems.

Table 3 shows the catalytic properties of the Ru catalysts in toluene hydrogenation. Similar trends were observed: Ru/C-silica (entry 1) was 12 times more active than Ru/C-silica-H (entry 2); Ru/AC1 (entry 3) was 11 times more active than Ru/AC1-H (entry 4); Ru/AC2 (entry 5) was 8 times more active than Ru/AC2-H (entry 6). Again, this indicates the high activity of thermally reduced Ru catalysts for aromatic hydrogenation with respect to hydrogen reduced analogues.

4. Discussion

The aforementioned results have demonstrated that thermally reduced Ru catalysts consistently exhibit remarkable catalytic activities and stabilities compared with their hydrogen-reduced counterparts. This is possibly because of intensive contact between the Ru metal and the carbon substrate (Ru−carbon) and enhanced hydrogen spillover effects, which could explain the superior catalytic activity observed even for larger Ru particles. In addition, the support pore structure and chemistry and catalyst particle size play an important role. Figure 9 illustrates schematically the environment for Ru nanoparticles supported on the various porous solids. As shown in Figure 9a, the hydrogen-reduced Ru nanoparticles are, in general, physically attached on a relatively flat surface in the support since the support is not actively involved the reduction reaction. In this case, the interfacial contact between the Ru nanoparticles and the substrate (either silica or carbon) could be regarded as a "point-contact" with a facet of the Ru nanocrystal. By contrast, in the thermal reduction process, the consumption of carbon species during Ru reduction results in a concave curvature in the carbon surface which allows the Ru nanoparticles to "burrow" and become semiembedded in the carbon matrix, as observed by TEM (Figures 2f and 3d). This creates many more Ru−carbon point contacts and thus forms a "surface-contact" on the carbon-coated silica support, as illustrated in Figure 9b, or on pure carbon supports, as shown in Figure 9c. This curvature in the surface contact plays an important role in enhancing metal−carbon interactions.[21−23] It is known that the interior concave surface of CNTs are electron-deficient, whereas the exterior convex surfaces are electron-rich;[23,32] this could strongly influence the electronic interaction of metal particles with the graphene sheets of CNTs. Recent redox studies showed that the encapsulation of transition metal nanoparticles such as iron within CNTs could retard the oxidation of these nanoparticles compared with nanoparticles supported on the outer convex CNT surface because of the specific metal−carbon electronic interactions imparted by the electron transfer between metal nanoparticles and the inner, electron-deficient CNT graphene sheets.[23] This stabilizes the metallic state of the transition metal. In our thermally reduced catalysts, the Ru nanoparticles are partially encapsulated in the carbon substrate

(32) Ugarte, D.; Chatelain, A.; de Heer, W. A. *Science* **1996**, *274*, 1897.

Table 2. Benzene Hydrogenation Activities of Various Supported Ru Catalysts

entry	Ru catalysts	Ru (wt %)	benzene:Ru[a]	*T* (°C)	*P* (H_2, MPa)	*t* (h)	conversn (%)[b]	activity × 10^{-3} (h^{-1})[c]
1	Ru/C-silica	4.2	10000:1	110	4.0	0.45	99.9	22.2
2	Ru/silica-H	6.6	2000:1	110	4.0	1.67	99.6	1.2
3	Ru/C-silica-H	5.4	2000:1	110	4.0	1.25	99.8	1.6
4	Ru/TMC	5.9	10000:1	110	4.0	0.51	99.9	19.6
5	Ru/TMC-H	5.8	2000:1	110	4.0	1.50	99.9	1.3
6	Ru/C-silica	4.2	20000:1	110	8.0	0.53	99.8	37.7
7	Ru/TMC	5.9	20000:1	110	8.0	0.60	99.9	33.3
8	Ru/AC1	5.3	10000:1	110	4.0	0.83	99.9	12.0
9	Ru/AC1-H	5.1	2000:1	110	4.0	2.00	53.4	0.5
10	Ru/AC2	5.5	10000:1	110	4.0	0.68	99.8	14.7
11	Ru/AC2-H	4.9	2000:1	110	4.0	1.25	99.9	1.6
12	Ru/XC	9.8	10000:1	110	4.0	0.90	99.8	11.1
13	Ru/XC-H	10.3	10000:1	110	4.0	2.00	69.9	3.5
14	Ru/C-silica (5th)	4.2	10000:1	110	4.0	0.48	99.9	20.8
15	Ru/TMC (5th)	5.9	10000:1	110	4.0	0.55	99.9	18.2
16	Ru/AC1 (5th)	5.3	10000:1	110	4.0	0.95	99.8	10.5
17	Ru/C-silica-AH	4.2	3000:1	110	4.0	1.21	99.8	2.5
18	Ru/TMC-AH	5.7	10000:1	110	4.0	0.82	99.9	12.2
19	RuC/silica	3.3	10000:1	110	4.0	0.67	99.9	14.9

[a] Molar ratio of benzene over Ru. [b] Conversion of benzene. [c] The activity was calculated as the conversion of mol of benzene/(mol of Ru/h).

Table 3. Toluene Hydrogenation Activities of Various Supported Ru Catalysts

entry	Ru catalysts	Ru (wt %)	toluene:Ru[a]	*T* (°C)	*P* (MPa)	*t* (h)	conversn (%)[b]	activity × 10^{-3} (h^{-1})[c]
1	Ru/C-silica	3.3	10000:1	110	4.0	1.02	99.8	9.8
2	Ru/C-silica-H	3.3	2000:1	110	4.0	2.00	82.8	0.8
3	Ru/AC1	5.3	10000:1	110	4.0	1.52	99.7	6.6
4	Ru/AC1-H	5.1	2000:1	110	4.0	2.00	61.3	0.6
5	Ru/AC2	5.5	10000:1	110	4.0	1.43	99.6	7.0
6	Ru/AC2-H	5.7	2000:1	110	4.0	2.00	91.3	0.9

[a] Molar ratio of toluene over Ru. [b] Conversion of toluene. [c] TOF was calculated as the conversion of mol of toluene/(mol of Ru/h).

within a concave surface (Figure 9b,c). By analogy with the CNT case, it can be postulated that the p_z orbit of graphene (π-bonded states) hybridizes strongly with the d orbitals of Ru. This hybridization would result in electron transfer from Ru to the graphene of the carbon substrate and would further impede the oxidation of Ru compared with those nanoparticles lying on a planar surface (Figure 9a). This interpretation is supported by XANES spectra analysis as shown in Figure 8. Moreover, the concave Ru−carbon contact may also strongly anchor and immobilize the Ru particles on the pore surface and prevent the Ru from leaching and migrating across the pore structure, thus agglomerating or coalescencing to form larger particles[15] which may block the pores and reduce catalytic activity. Table S1 shows that leaching of fresh thermally reduced catalysts Ru/C-silica (entry 1) and Ru/AC1 (entry 2) is much lower than observed for hydrogen-reduced Ru/silica-H (entry 3), Ru/C-silica-H (entry 4), and Ru/AC1-H (entry 5). Similarly, the leaching of thermally reduced single-use Ru catalysts after 4-days shaking in water was still lower than for the hydrogen-reduced counterparts (Table S1; entries 6−9). Moreover, no aggregation of Ru nanoparticles was observed after five reaction runs for the thermally reduced catalysts (Figure S3). These observations may support the presence of strong multipoint interactions between the Ru nanoparticles and the carbon substrates.

Hydrogenation of benzene and toluene typically involves hydrogen spillover mechanisms.[33,34] It is known that hydrogen molecules may be dissociatively adsorbed on the Ru surface[35] and spilled over from the Ru particles onto the support and that the aromatic compounds are often found to be adsorbed on the surface of the support.[34,36] The single point-contact discussed above has been referred to as the "narrow road" and is believed to limit the transfer of hydrogen spillover species (H_{so}) from Ru particles onto the support, thus leading to a lower catalytic activity in the catalysts. The much more extensive Ru−carbon surface contacts produced in the thermal reduction approach might widen this "road" and facilitate the transport of H_{so} from the Ru particles to the support for hydrogen spillover and hydrogenation reactions.[20,37] To test this assumption, we calcined Ru/C-silica and Ru/TMC in air at 200 °C by moderate oxidation of Ru nanoparticles (see XRD pattern of Ru/C-silica-A in Figure 5 and TG curves in Figure 7) followed by hydrogen reduction to produce Ru/C-silica-AH and Ru/TMC-AH, respectively. No significant change in the Ru particle morphology (e.g., degree of interfacial surface contact) was observed by TEM before and after calcination (Figure 4), and the nature of the surface contact is believed to be maintained after calcination/reduction. The Ru nanoparticle surface chemistry state on Ru/C-silica-AH and Ru/

(33) (a) Conner, W. C., Jr.; Falconer, J. L. *Chem. Rev.* **1995**, *95*, 759. (b) Li, C., Xin, Q., Eds. *Studies in Surface Science Catalysis 112*; Elsevier Science BV: Amsterdam, 1997.

(34) (a) Lin, S. D.; Vannice, M. A. *J. Catal.* **1993**, *143*, 539. (b) Lin, S. D.; Vannice, M. A. *J. Catal.* **1993**, *143*, 554. (c) Lin, S. D.; Vannice, M. A. *J. Catal.* **1993**, *143*, 563. (d) Ioannides, T.; Verykios, X. E. *J. Catal.* **1993**, *143*, 175.

(35) Parmeter, J. E.; Hills, M. M.; Weinberg, W. H. *J. Am. Chem. Soc.* **1987**, *109*, 72.

(36) (a) King, T. S.; Wu, X.; Gerstein, B. C. J. *Am. Chem. Soc.* **1986**, *108*, 6056. (b) Badenes, P.; Daza, L.; Rodriguez-Ramos, I.; Guerrero-Ruiz, A. *Stud. Surf. Sci. Catal.* **1997**, *112*, 241. (c) Ishikawa, H.; Kondo, J. N.; Domen, K. *J. Phys. Chem. B* **1999**, *103*, 3229.

(37) (a) Boudart, M.; Aldag, A. W.; Vannice, M. A. *J. Catal.* **1970**, *18*, 46. (b) R. B. Levy, M. Boudart, *J. Catal.* **1974**, *32*, 304. (c) Srinivas, S. T.; Rao, P. K. *J. Catal.* **1994**, *148*, 470. (d) Lueking, A.; Yang, R. T. *AIChE J.* **2003**, *49*, 1556. (e) Lachawiec, A. J., Jr.; Qi, G.; Yang, R. T. *Langmuir* **2005**, *21*, 11418. (f) Ansón, A.; Lafuente, E.; Urriolabeitia, E.; Navarro, R.; Benito, A. M.; Maser, W. K.; Martínez, M. T. *J. Phys. Chem. B* **2006**, *110*, 6643. (g) Jain, P.; Fonseca, D. A.; Schaible, E.; Lueking, A. D. *J. Phys. Chem. C* **2007**, *111*, 1788.

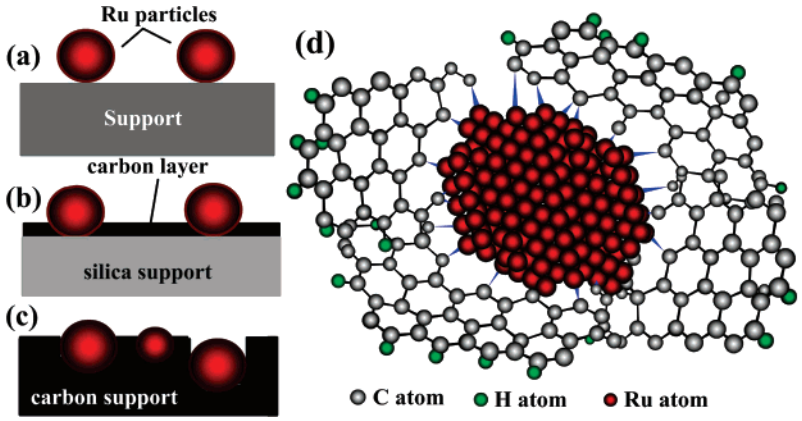

Figure 9. Schematic representation of Ru nanoparticles on the various supports: (a) hydrogen-reduced Ru nanoparticles attached on the support surface; (b) thermally reduced Ru nanoparticles sitting on the C-silica support; (c) thermally reduced Ru nanoparticles sitting in a carbon support; (d) Ru−C linkages formed between a Ru nanoparticle and the edge of graphene (blue arrows).

TMC-AH should be similar to that of Ru/C-silica-H and Ru/TMC-H. As such, the higher activities observed for Ru/C-silica-AH and Ru/ TMC-AH (Table 2, entries 17 and 18) with respect to Ru/C-silica-H and Ru/TMC-H (Table 2, entries 3 and 5) suggests indirectly that the nature of the Ru−carbon interfacial interaction may be responsible for the enhanced catalytic activity rather than large differences in particle surface chemistry for materials produced by the two different routes.

Nonetheless, the catalytic activities for the Ru/C-silica-AH and Ru/TMC-AH catalysts are still much lower than those of their parent materials, Ru/C-silica and Ru/TMC, implying that factors besides the extensive Ru−carbon surface contact are also responsible for the enhanced activity. It is known that multiple bonds between Ru atoms and carbon atoms (Ru−C) can be created on the Ru metal surfaces to form Ru−surface carbene complexes,[38,39] thus providing chemically reactive sites and an efficient conduit for charge carriers.[39] The high-temperature thermal treatment in nitrogen gas might break the C−C, C−H, C−O, and C═C bonds in graphene layers of the carbon substrate near surface of Ru nanoparticles, therefore leaving unsaturated carbon atoms at the graphene layer edges (defects). These unsaturated carbon atoms may be coordinated with surface unsaturated Ru atoms to form Ru−C chemical linkages as shown in Figure 9d. These linkages are analogous to those that occur between heterocyclic compounds and transition metals to form a strong heterocycle−metal bonding in polymer and carbon substrates[40,41] and could result in both the stabilization of the Ru nanoparticles and also a rapid transfer of H_{so}, electrons, and charges[39,42] from the Ru particles to the support surface. We suggest that the tremendous decrease in activity of Ru/C-silica-AH and Ru/TMC-AH catalysts compared with that of Ru/C-silica and Ru/TMC is linked to the lack of such Ru−C linkages which are severed by the calcination process in air and not restored by hydrogen reduction. Moreover, thermally reduced catalysts such as Ru/TMC also displayed a strong oxidation resistance, as observed by XANES spectral analysis (Figure 8), possibly indicating the presence of surface Ru−C linkages that make the saturated Ru surface more stable. In addition, the reduced leaching observed for thermally reduced catalysts (Table S1) may also be related to these chemical linkages. Other factors may contribute to the enhanced activity; for example, the amount of exposed Ru surface, the particle size, and carbon−substrate surface properties. Following methods similar to those reported previously[19a] and using the thermal reduction process, we found Ru catalysts with Ru nanoparticles embedded in a templated carbon matrix to exhibit a much lower activity (2.8×10^3 h^{-1}) than that of Ru/TMC due to the inaccessibility of the majority of Ru nanoparticles that were fully buried in the templated carbon framework, indicating the importance of retaining an exposed Ru surface. Ab initio calculation and experimental results have demonstrated that the lack of active sites on small Ru nanoparticles is responsible for their low catalytic activity and that activity can be increased by sintering the small Ru nanoparticles in a supported catalyst;[43] this is consistent with our observations. It has also been found that the chemisorption of dissociative hydrogen is very slow or inhibited on oxygen-adsorbed Ru surfaces.[44] In our work, the thermally reduced Ru/TMC catalysts with a higher resistance against oxidation than hydrogen-reduced catalysts should provide the hydrogen species more rapidly for hydrogenation. It should be noted that the presence of residual chlorine species when using a cheap Ru chlorine salt as a catalyst precursor always blocks or poisons the active Ru surface to some degree and that removing these species by hydrogen reduction is difficult.[45] High-temperature thermal reduction (900 °C) could completely remove the chlorine species on the Ru surface[46] and also leads to full reduction of metallic Ru. In contrast, hydrogen reduction could not be carried out to completion at high

(38) (a) George, P. M.; Avery, N. R.; Weinberg, W. H.; Tebbe, F. N. *J. Am. Chem. Soc.* **1983**, *105*, 1393. (b) Gunia, M.; Jakob, P.; Sander, W.; Woell, C. *J. Phys. Chem. B* **2004**, *108*, 14025. (c) Chen, W.; Davies, J. R.; Ghosh, D.; Tong, M. C.; Konopelski, J. P.; Chen, S. *Chem. Mater.* **2006**, *18*, 5253.
(39) Tulevski, G. S.; Myers, M. B.; Hybertsen, M. S.; Steigerwald, M. L.; Nuckolls, C. *Science* **2005**, *309*, 591.
(40) Yuasa, M.; Yamaguchi, A.; Itsuki, H.; Tanaka, K.; Yamamoto, M.; Oyaizu, K. *Chem. Mater.* **2005**, *17*, 4278.
(41) Bashyam, R.; Zelenay, P. *Nature* **2006**, *443*, 63.
(42) Roland, U.; Braunschweig, T.; Roessner, F. *J. Mol. Catal., A* **1997**, *127*, 61.
(43) (a) Jacobsen, C. J. H.; Dahl, S.; Hansen, P. L.; Törnqvist, E.; Jensen, L.; Topsøe, H.; Prip, D. V.; Møenshaug, P. B.; Chorkendorff, I. *J. Mol. Catal., A* **2000**, *163*, 19. (b) Liang, C.; Wei, Z.; Xin, Q.; Li, C. *Appl. Catal., A* **2001**, *208*, 193. (c) Honkala, K.; Hellman, A.; Remediakis, I. N.; Logadottir, A.; Carlsson, A.; Dahl, S.; Christensen, C. H.; Nørskov, J. K. *Science* **2005**, *307*, 555.
(44) (a) Shi, S.-K.; Schreifels, J. A.; White, J. M. *Surf. Sci.* **1981**, *105*, 1. (b) Hrbek, J. *J. Phys. Chem.* **1986**, *90*, 6217.
(45) (a) Tiep, L. V.; Tardy, M. B.; Bugli, G.; Djega-Mariadassou, G.; Che, M.; Bond, G. C. *J. Catal.* **1986**, *99*, 449. (b) Wu, X.; Gerstein, B. C.; King, T. S. *J. Catal.* **1992**, *135*, 68.
(46) Hájek, J.; Kumar, N.; Mäki-Arvela, P.; Salmi, T.; Murzin, D. Y.; Paseka, I.; Heikkilä, T.; Laine, E.; Laukkanen, P.; Väyrynen, J. *Appl. Catal., A* **2003**, *251*, *385*.

temperatures because methanation and gasification of carbon catalyzed by Ru starts at about 400 °C.[27] In addition, the reduction of surface-oxygen functional groups on the carbon substrate at high temperatures in nitrogen gas[47] could increase the hydrogenation rate of the C=C bond.[48]

The presence of carbon species as a reducing species is a prerequisite in thermal reduction at high temperatures as shown in Figure 5. The enhanced activity of Ru/C-silica catalysts suggests that structured solids such as honeycomb inorganic monoliths or ceramic foams, which have been widely employed as catalyst supports in the past, could also be used as Ru catalyst substrates after carbon coating. We have also demonstrated the effectiveness of such methods using an industrial alumina catalyst support (data not shown here). Experiments were also conducted where we added a small amount of sucrose (a carbon reductant precursor) in the Ru precursor solution to impregnate the porous silica, followed by thermal reduction at 900 °C for 2 h in nitrogen to prepare RuC/silica catalyst. The hydrogenation activity of this material (Table 2, entry 19) was also much higher than for Ru/silica-H and Ru/C-silica-H but a little lower than that observed for Ru/C-silica. This suggests, for example, that surfactants utilized as organic templates for the synthesis of porous silica might also be used as carbon precursors to obtain thermally reduced Ru nanoparticles. A large number of silica−carbon or silica−polymer composites recently developed[49] could also be good supports for this thermal reduction method, as might dendrimer-encapsulated Ru nanoparticles or organometallic Ru complexes dispersed in the pores of inorganic porous materials. Future research work will focus on the control of Ru particle size, the precise identification of the nature of the Ru−C linkages, and the hydrogen spillover mechanism and also investigation of different heteroatom-doped carbon precursors. For example, Ru nanoparticles might be coordinated with N to form Ru−N coordination bonds and hence facilitate the catalytic activity.[50] Other potential applications, such as hydrogen storage enhanced by hydrogen spillover effect,[51] ammonia synthesis,[43] and selective hydrogenation,[14] are also future targets of exploration for our thermal reduction methods.

5. Conclusions

In summary, we have demonstrated a simple and versatile thermal reduction method for preparing highly active heterogeneous Ru catalysts for the hydrogenation of monoaromatics. The investigation of Ru nanoparticles supported on various substrates, including mesoporous silica SBA-15, surface-carbon-coated SBA-15, templated mesoporous carbon, activated carbon, and carbon black, demonstrate significant advantages for the thermal reduction method. It was observed that thermally reduced Ru nanoparticles possessed a high degree of dispersion, appropriate particle size, high crystallinity, strong resistance against oxidation, reduced leaching, and hence high catalytic activities and stabilities in the hydrogenation of benzene and toluene. The thermal reduction method described in this work allows us to maximize the efficient usage of the precious Ru metal for a variety of sustainable technology applications.

Acknowledgment. We gratefully acknowledge the National University of Singapore for funding the work with Grant No. R279000217123 and the Engineering and Physical Sciences Research Council (EPSRC, EP/C511794/1) for funding.

Supporting Information Available: N_2 adsorption−desorption isotherms and PSD of the Ru catalysts, a TEM image of RuO_2/silica, an STEM image of Ru/C-silica, a TEM image of Ru/TMC after five uses, and complete ref 26. This material is available free of charge via the Internet at http://pubs.acs.org.

JA072697V

(47) Su, F.; Lv, L.; Tee, M. H.; Zhao, X. S. *Carbon* **2005**, *43*, 1156.
(48) (a) Toebes, M. L.; Prinsloo, F. F.; Bitter, J. H.; Jos, van Dillen, A.; de Jong, K. P. *J. Catal.* **2003**, *214*, 78. (b) Bachiller-Baeza, B.; Guerrero-Ruiz, A.; Rodríguez-Ramos, I. *Appl. Catal., A* **2000**, *192*, 289.
(49) (a) Deng, Y.; Yu, T.; Wan, Y.; Shi, Y.; Meng, Y.; Gu, D.; Zhang, L.; Huang, Y.; Liu, C.; Wu, X.; Zhao, D. *J. Am. Chem. Soc.* **2007**, *129*, 1690. (b) Wu, S.; Ju, H.; Liu, Y. *Adv. Funct. Mater.* **2007**, *17*, 585. (c) Hu, Q.; Kou, R.; Pang, J.; Ward, T. L.; Cai, M.; Yang, Z.; Lu, Y.; Tang, J. *Chem. Commun.* **2007**, 601. (d) Pang, J.; John, V. T.; Loy, D. A.; Yang, Z.; Lu, Y. *Adv. Mater.* **2005**, *17*, 704. (e) Choi, M.; Kleitz, F.; Liu, D.; Lee, H. Y.; Ahn, W. -S.; Ryoo, R. *J. Am. Chem. Soc.* **2005**, *127*, 1924.
(50) (a) Goettmann, F.; Fischer, A.; Antonietti, M.; Thomas, A. *Angew. Chem., Int. Ed.* **2006**, *45*, 4467. (b) Miyazaki, S.; Ohkubo, K.; Kojima, T.; Fukuzumi, S. *Angew. Chem., Int. Ed.* **2007**, *46*, 905.
(51) (a) Lueking, A.; Yang, R. T. *J. Catal.* **2002**, *206*, 165. (b) Lueking, A.; Yang, R. T. *Appl. Catal., A* **2004**, *265*, 259. (c) Li, Y.; Yang, R. T. *J. Am. Chem. Soc.* **2006**, *128*, 726. (d) Li, Y.; Yang, R. T. *J. Am. Chem. Soc.* **2006**, *128*, 8136.